

**This is a self-archived version of an original article. This version may differ from the original in pagination and typographic details.**

**Author(s):** Lahtinen, Elmeri; Kukkonen, Esa Petteri; Jokivartio, Joonas; Parkkonen, Joni; Virkajärvi, Jussi; Kivijärvi, Lauri; Ahlskog, Markus; Haukka, Matti

**Title:** Preparation of Highly Porous Carbonous Electrodes by Selective Laser Sintering

**Year:** 2019

**Version:** Published version

**Copyright:** © 2019 American Chemical Society

**Rights:** CC BY 4.0

**Rights url:** <http://rightsstatements.org/page/InC/1.0/?language=en>

**Please cite the original version:**

Lahtinen, E., Kukkonen, E. P., Jokivartio, J., Parkkonen, J., Virkajärvi, J., Kivijärvi, L., Ahlskog, M., & Haukka, M. (2019). Preparation of Highly Porous Carbonous Electrodes by Selective Laser Sintering. *ACS Applied Energy Materials*, 2(2), 1314-1318.  
<https://doi.org/10.1021/acsaem.8b01881>

## Preparation of Highly Porous Carbonous Electrodes by Selective Laser Sintering

Elmeri Lahtinen, Esa Kukkonen, Joonas Jokivartio, Joni Parkkonen, Jussi Virkajärvi, Lauri Kivijärvi, Markus Ahlskog, and Matti Haukka

*ACS Appl. Energy Mater.*, **Just Accepted Manuscript** • DOI: 10.1021/acsaem.8b01881 • Publication Date (Web): 10 Jan 2019

Downloaded from <http://pubs.acs.org> on January 14, 2019

### Just Accepted

“Just Accepted” manuscripts have been peer-reviewed and accepted for publication. They are posted online prior to technical editing, formatting for publication and author proofing. The American Chemical Society provides “Just Accepted” as a service to the research community to expedite the dissemination of scientific material as soon as possible after acceptance. “Just Accepted” manuscripts appear in full in PDF format accompanied by an HTML abstract. “Just Accepted” manuscripts have been fully peer reviewed, but should not be considered the official version of record. They are citable by the Digital Object Identifier (DOI®). “Just Accepted” is an optional service offered to authors. Therefore, the “Just Accepted” Web site may not include all articles that will be published in the journal. After a manuscript is technically edited and formatted, it will be removed from the “Just Accepted” Web site and published as an ASAP article. Note that technical editing may introduce minor changes to the manuscript text and/or graphics which could affect content, and all legal disclaimers and ethical guidelines that apply to the journal pertain. ACS cannot be held responsible for errors or consequences arising from the use of information contained in these “Just Accepted” manuscripts.



# Preparation of Highly Porous Carbonous Electrodes by Selective Laser Sintering

*Elmeri Lahtinen, Esa Kukkonen, Joonas Jokivartio, Joni Parkkonen, Jussi Virkajärvi,*

*Lauri Kivijärvi, Markus Ahlskog and Matti Haukka \**

E. Lahtinen, E. Kukkonen, L. Kivijärvi, Prof. M. Haukka

Department of Chemistry, University of Jyväskylä, P.O. Box 35, FI-40014 Jyväskylä,  
Finland

J. Jokivartio, Prof. M. Ahlskog

Department of Physics, Nanoscience Center, University of Jyväskylä, P.O. Box 35, FI-  
40014 Jyväskylä, Finland

J. Parkkonen, Dr. J. Virkajärvi

Department of Physics, University of Jyväskylä, P.O. Box 35, FI-40014 Jyväskylä, Finland

**Keywords:** Porous Electrodes, 3D printing, Selective Laser Sintering, Conductivity,

Graphite

1  
2  
3  
4  
5  
6  
7  
8  
9  
10  
11  
12  
13  
14  
15  
16  
17  
18  
19  
20  
21  
22  
23  
24  
25  
26  
27  
28  
29  
30  
31  
32  
33  
34  
35  
36  
37  
38  
39  
40  
41  
42  
43  
44  
45  
46  
47  
48  
49  
50  
51  
52  
53  
54  
55  
56  
57  
58  
59  
60

**Abstract**

Selective Laser Sintering (SLS) 3D printing was utilized to fabricate highly porous carbonous electrodes. The electrodes were prepared by using a mixture of fine graphite powder and either polyamide-12, polystyrene or polyurethane polymer powder as SLS printing material. During the printing process the graphite powder was dispersed uniformly on the supporting polymer matrix. Graphite's concentration in the mixture was varied between 5 and 40 wt-% to find the correlation between the carbon content and conductivity. The graphite concentration, polymer matrix and the printing conditions all had an impact on the final conductivity. Due to the SLS printing technique, all the 3D printed electrodes were highly porous. By using polyurethane as the supporting matrix it was possible to produce flexible electrodes in which the conductivity is sensitive to pressure and mechanical stress. Physical properties such as graphite distribution, attachment and the overall porosity of the printed electrodes were studied using scanning electron microscopy (SEM), helium ion microscopy (HIM) and X-ray tomography. The results show that the combination of chemical design of the printing material and the

1  
2  
3 utilization of SLS 3D printing enables fabrication of highly customizable electrodes with  
4  
5  
6  
7 desired chemical, physical, mechanical, and flow-through properties.  
8  
9

## 10 11 12 **Introduction** 13

14  
15  
16 Increasing demand for high performance batteries in wide variety of electronic  
17  
18 applications from portable electronic devices to electric cars has generated a need for  
19  
20 new approaches in battery design.<sup>1,2</sup> Especially the development of novel electrodes has  
21  
22  
23 gained a lot of interest.<sup>3-5</sup> Obviously, the most important property of an electrode is its  
24  
25  
26 conductivity but other features such as surface area and porosity can also have a  
27  
28  
29 significant impact on the electrodes' electrochemical properties and their applicability from  
30  
31  
32 more conventional systems to redox flow batteries.<sup>6</sup> When considering a typical graphite  
33  
34  
35 electrode, the achievable surface area consists only of the outer layer of the electrode the  
36  
37  
38 inner parts of the electrode are not accessible. Several methods to increase the surface  
39  
40  
41 area have been proposed, including the addition of nanomaterials into the graphite, the  
42  
43  
44 usage of different templating methods and the use of organic monolayered additives.<sup>7-12</sup>  
45  
46  
47  
48  
49  
50  
51  
52  
53  
54  
55  
56  
57  
58  
59  
60

1  
2  
3  
4 During the last decade, three-dimensional printing has also been exploited in fabrication  
5  
6  
7 of highly customizable electrochemical devices.<sup>13,14</sup> Several papers have been published  
8  
9  
10 for example of 3D printed graphene-based electrodes and microbatteries.<sup>15–20</sup> In these  
11  
12  
13  
14 studies, three-dimensional printing has enabled a rapid production of components and  
15  
16  
17 devices for electrochemical applications. However, in most cases the 3D printing  
18  
19  
20  
21 technique used has been either Fused Deposition Modeling (FDM) or Direct Ink Writing  
22  
23  
24 (DIW), while other 3D printing techniques have received little to no interest. Both FDM  
25  
26  
27  
28 and DIW produce surfaces that are not inherently porous and the methods often require  
29  
30  
31 specifically customized printing materials. In principle, a wide range of commercial  
32  
33  
34  
35 materials are available but fine-tuning these printing materials for specific applications  
36  
37  
38 while simultaneously trying to match the requirements of a specific printing method can  
39  
40  
41  
42 be laborious and demanding. From this point of view powder-based methods, such as  
43  
44  
45 Selective Laser Sintering (SLS), can provide a way to avoid some of these pitfalls. For  
46  
47  
48  
49 example, with the SLS 3D printing technique, it is possible to produce objects that are  
50  
51  
52 inherently porous. In SLS printing, small particles with a typical diameter of 50–100  $\mu\text{m}$   
53  
54  
55  
56 are fused together by laser which gives, at least up to a point, control over the physical  
57  
58  
59  
60

1  
2  
3 characteristics such as the porosity and mechanical strength of the material by fine-tuning  
4  
5  
6  
7 the printing parameters such as laser power, exposure time and printing temperature.<sup>21–</sup>  
8

9  
10 <sup>24</sup> When the particles are sintered in such a way that only their surfaces are partially  
11  
12  
13  
14 melted, a solid structure containing accessible voids between the sintered grains is  
15  
16  
17  
18 obtained. With powder-based methods, it is also relatively easy to add functional additives  
19  
20  
21 into the printed object by simply mixing the additive with the printable matrix. If the matrix  
22  
23  
24 particles are only partially sintered, the additive is dispersed on the surface of these  
25  
26  
27  
28 particles and therefore accessible by fluids flowing through the printed object enabling  
29  
30  
31 applications such as porous flow-through columns for scavenging metal ions from  
32  
33  
34 aqueous solutions.<sup>25</sup> The SLS technique also allows the alteration of physical properties  
35  
36  
37  
38 such as the density of the printed objects within the object itself. This means that different  
39  
40  
41 areas of the 3D printed object can be tuned to have different porosities and objects with  
42  
43  
44 well-defined permeable and impermeable areas can be made.<sup>25</sup> This in turn broadens the  
45  
46  
47  
48 range of plausible applications for the printed objects.  
49

50  
51  
52 In SLS 3D printing, the most commonly used printing materials are simple polymers  
53  
54  
55  
56 such as polyamides, polypropylene or polystyrene. These polymers are nonconductive  
57  
58  
59



1  
2  
3 by nature and therefore not suitable as electrode materials. Obviously, conducting  
4  
5  
6  
7 polymers could be used to obtain electrodes. However, the chemical nature of the  
8  
9  
10 electrode is also dependent of the material. Furthermore, the conductive polymers are  
11  
12  
13 often relatively expensive.<sup>26</sup> Therefore, use of a conductive component only as an additive  
14  
15  
16 seems like an appealing option. The SLS technique sets only minimal requirements for  
17  
18  
19 the choice of the functional additives as nearly any components can be mixed within the  
20  
21  
22 matrix powder. There is a wide range of different conductive components available, from  
23  
24  
25  
26  
27  
28 conductive polymers to carbon nanotubes and metals, which could potentially be used as  
29  
30  
31  
32  
33  
34  
35  
36  
37  
38  
39  
40  
41  
42  
43  
44  
45  
46  
47  
48  
49  
50  
51  
52  
53  
54  
55  
56  
57  
58  
59  
60

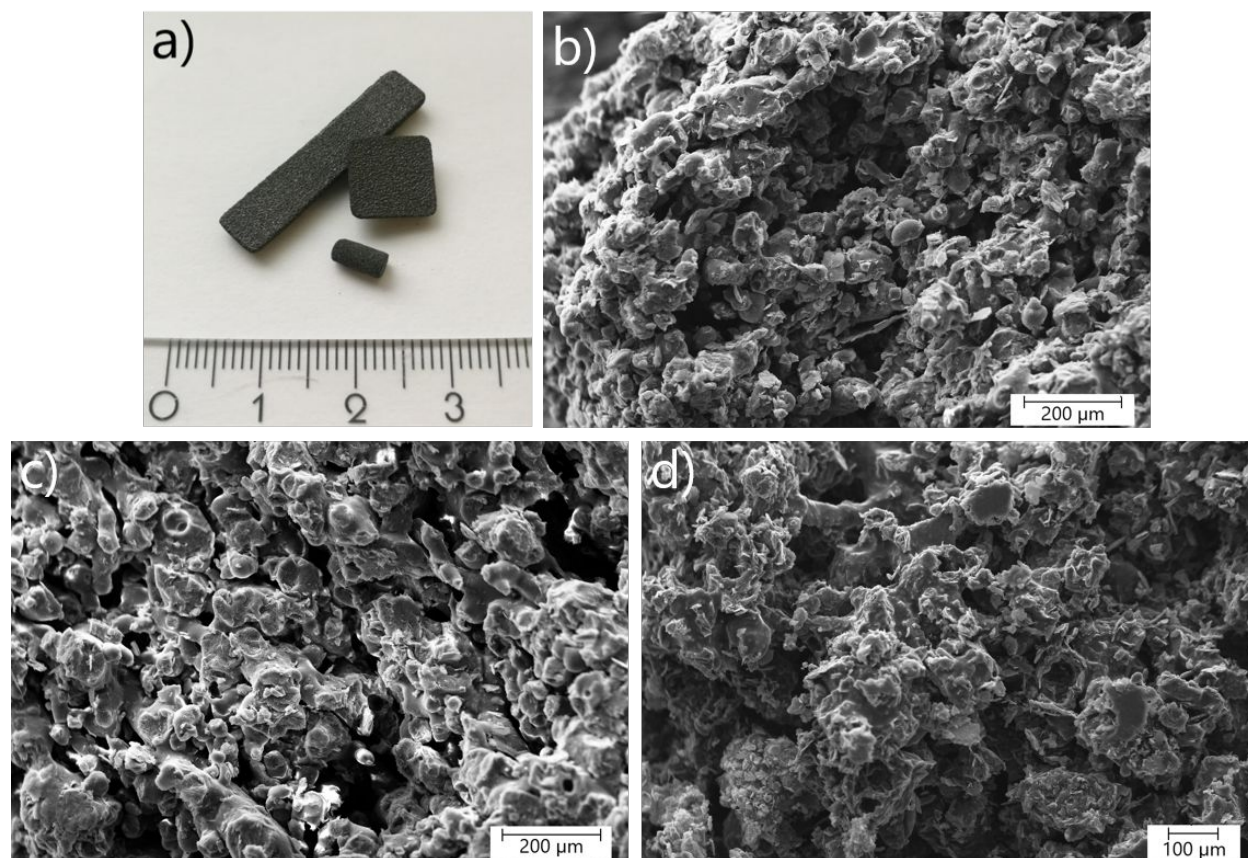
conductive additives. Simple graphite, however, is a good example of an additive that possesses conductivity and is still rather cost-efficient. In this work, graphite powder mixed into either polyamide-12, polystyrene or polyurethane matrix was used for preparation of highly porous carbonous electrodes using SLS 3D printing. The graphite content plays key role in the conductivity and therefore the impact of the graphite concentration was investigated to find the optimum graphite/matrix ratio.

## Results and Discussion

1  
2  
3  
4 The printing material for the fabrication of the electrodes was prepared by mixing either  
5  
6  
7 commercial polystyrene, polyamide-12 or polyurethane powder with synthetic bulk  
8  
9  
10 graphite powder. The graphite content was varied between 5 and 40 wt-% to find the  
11  
12  
13 optimum additive/matrix ratio. Electrodes with different shapes and sizes were designed  
14  
15  
16 for different analytical experiments. Square and rectangle-shaped electrodes (Fig. 1 a)  
17  
18 were used for the resistance measurements and for performing the Helium Ion  
19  
20  
21 Microscopy (HIM)<sup>27</sup> and the Scanning Electron Microscopy (SEM) imaging, whereas  
22  
23  
24 cylinder shaped electrodes (Fig. 1 a) were prepared for the X-ray tomography analysis.  
25  
26  
27  
28 Physical properties of the electrodes were fine-tuned by optimizing printing parameters  
29  
30  
31 such as layer thickness, laser power and printing speed.  
32  
33  
34  
35  
36  
37

38 The amount of graphite in the powder mixture affects the required printing parameters.  
39  
40  
41 To obtain electrodes with sufficient mechanical strength and durability while retaining the  
42  
43  
44 porous structure requires adjusting the printing conditions for each graphite/matrix  
45  
46  
47 system. The structure of the printed electrodes and the distribution of graphite were  
48  
49  
50 studied using SEM, HIM and X-ray tomography. The SEM images of the break surfaces  
51  
52  
53 of the 3D printed graphite/polystyrene electrodes are shown in Fig. 1 b, c and d. The set  
54  
55  
56  
57  
58  
59  
60

1  
2  
3 of SEM images of the graphite/polyamide-12 electrodes also display similar structural  
4 characteristics (Figures S1-S4). The images reveal the highly macroporous structure of  
5  
6 the material, in which the graphite powder is distributed evenly throughout the objects. As  
7  
8  
9  
10  
11  
12  
13  
14 can be seen, the polymer particles have been only partially fused together by the sintering  
15  
16  
17 process, thus forming the porous structure with accessible voids between the particles.  
18  
19  
20



48 Figure 1. Rectangle, square and cylinder-shaped, polystyrene-based SLS 3D printed  
49 electrodes with 30 wt-% of graphite (a). SEM image of the break surface of 3D printed  
50 polystyrene electrode with 20 wt-% (b), 30 wt-%(c) and 40 wt-% (d) of graphite.  
51  
52  
53  
54  
55  
56  
57  
58  
59  
60

1  
2  
3  
4 To avoid any problems caused by possible charging of the material during the SEM  
5  
6  
7 imaging, the 3D printed electrodes were also analyzed by Helium Ion Microscopy (Fig.  
8  
9  
10 2). The HIM images confirmed the highly macroporous structure of the electrodes, but  
11  
12  
13 they also clearly show graphite's attachment on the surface of the polymeric three-  
14  
15  
16 dimensional network (Fig. 2 a). In the SLS 3D printing process, it is possible to obtain  
17  
18  
19 objects where the additive is not entirely encapsulated by the matrix but it is firmly attached  
20  
21  
22 only on the matrix's partially melted surface of the polymer matrix. This means that the  
23  
24  
25 additive is not just loosely trapped within the three-dimensional structure, it is strongly  
26  
27  
28 anchored onto the polymeric matrix. On the other hand, the additive is achievable by  
29  
30  
31 fluids, gases or liquids, passing through the porous material.  
32  
33  
34  
35  
36  
37  
38  
39  
40  
41  
42  
43  
44  
45  
46  
47  
48  
49  
50  
51  
52  
53  
54  
55  
56  
57  
58  
59  
60

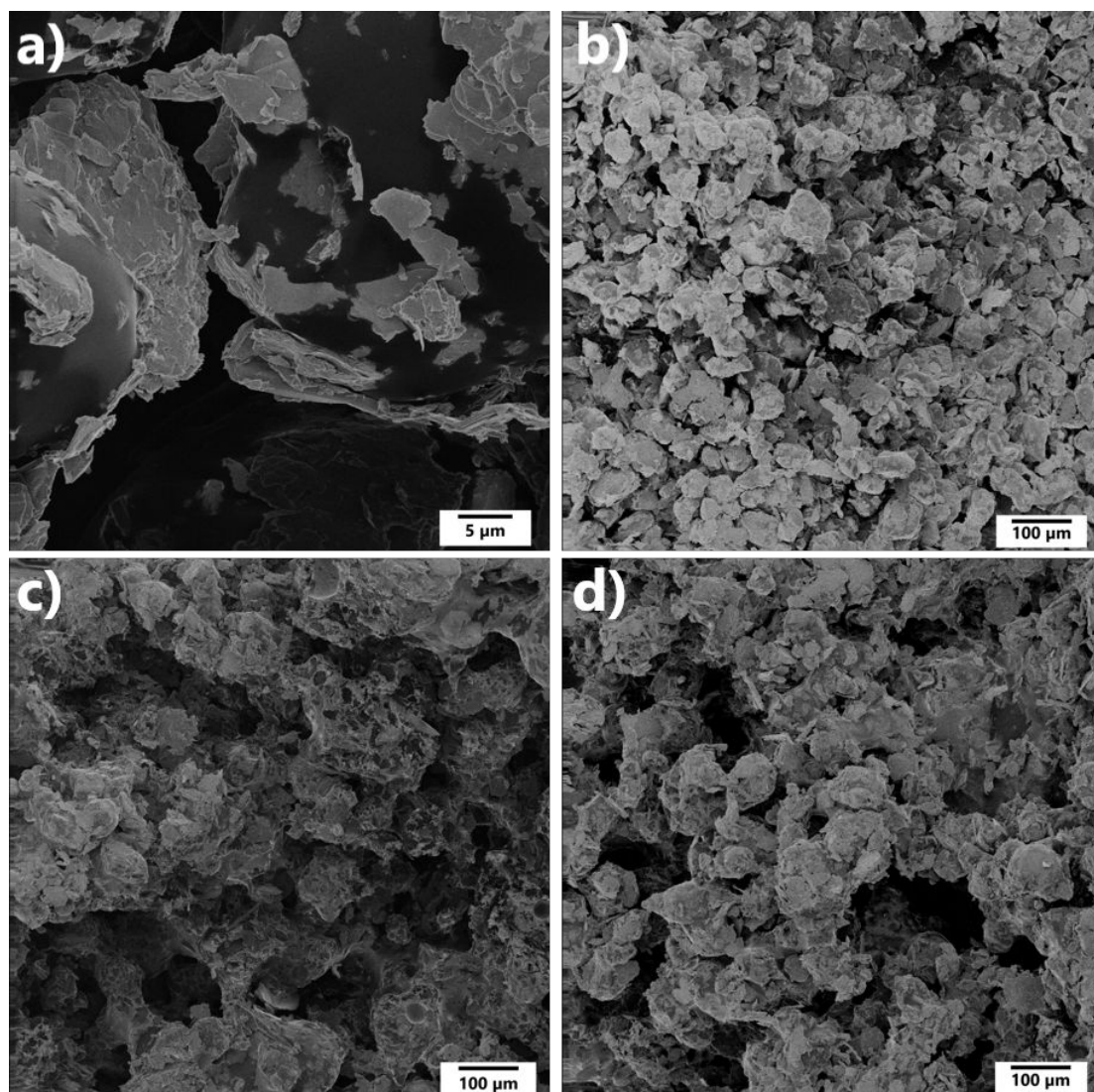


Figure 2. Helium Ion Microscope (HIM) image of the break surface of the 3D printed polystyrene electrode having 20 wt-% of graphite, showing that the graphite flakes are covering the surface of the partially melted polystyrene matrix (a). HIM image of the break surface of the 3D printed polystyrene electrode with 20 wt-% (b), 30 wt-%(c) and 40 wt-% (d) of graphite.

1  
2  
3  
4  
5  
6  
7 To confirm that the images of the outer layer and the break surfaces obtained via HIM  
8  
9  
10 and SEM imaging represent the overall internal structure of the electrodes, X-ray  
11  
12  
13 tomography of the electrodes was carried out. For these analyses, electrodes with 30 wt-  
14  
15  
16 % of graphite were used. The tomography images (Fig. 3) show that the whole electrode  
17  
18  
19 is porous and that the structure observed from the HIM and the SEM images describe the  
20  
21  
22 structure well. The structural analyses confirmed that porous electrodes can be obtained  
23  
24  
25 with both polystyrene and polyamide-12. The detailed analysis of the X-ray tomography  
26  
27  
28 results showed that the macroporous structure of the polystyrene electrode has 41 % of  
29  
30  
31 empty space inside the electrode whereas the polyamide-12 based electrode has 49 %  
32  
33  
34 of empty space. Analysis of the average pore diameter indicated that the polystyrene and  
35  
36  
37 polyamide-12 electrodes have average pore diameters between 10-55  $\mu\text{m}$  and 10-75  $\mu\text{m}$ ,  
38  
39  
40  
41 respectively (Fig. S5 and S6).  
42  
43  
44  
45  
46  
47  
48  
49  
50  
51  
52  
53  
54  
55  
56  
57  
58  
59  
60

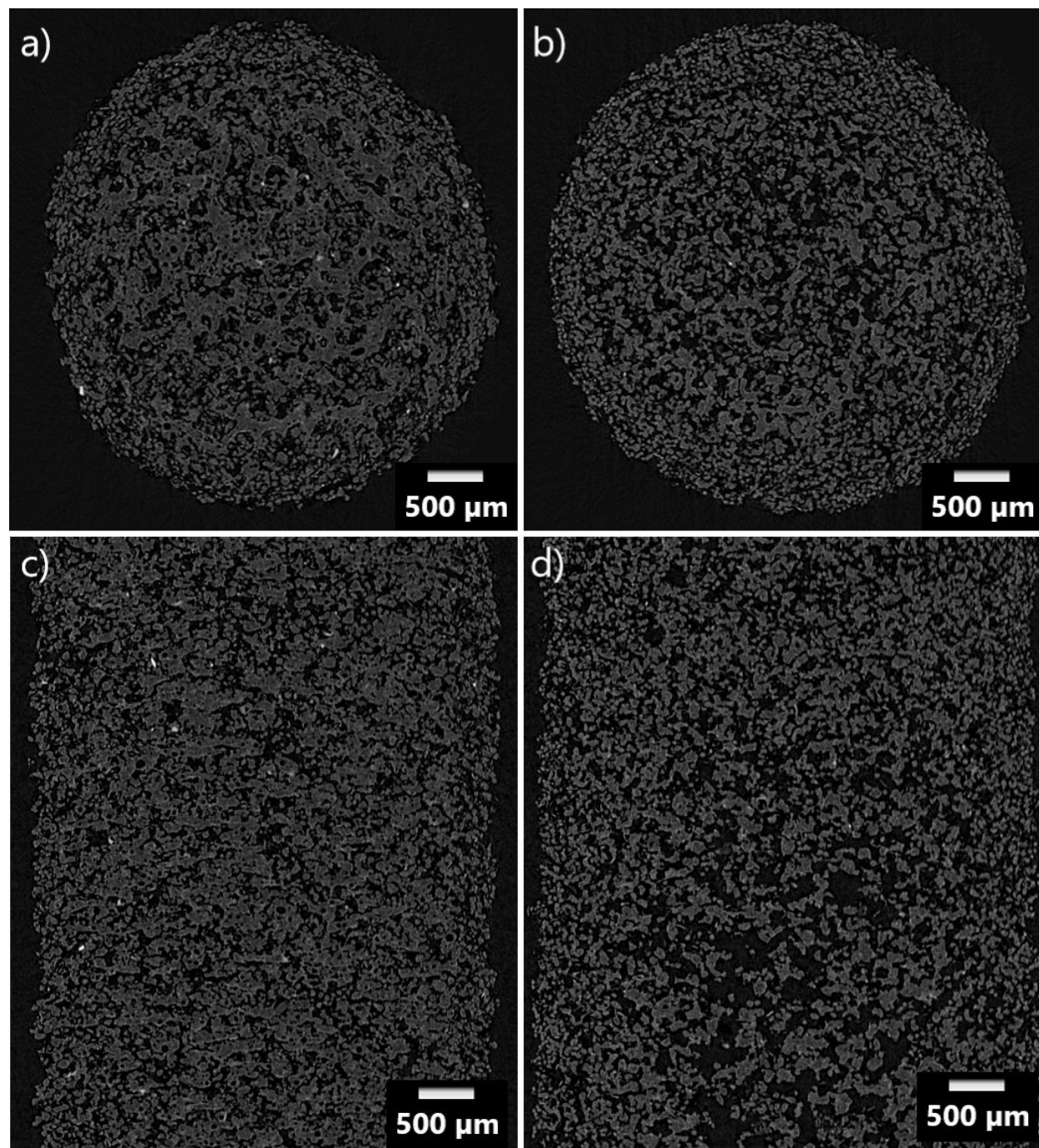


Figure 3. Horizontal slice of the structure of the cylinder shaped SLS printed electrode from X-ray tomography analysis of polystyrene (a) and polyamide-12 (b) based electrodes



1  
2  
3  
4 having 30 wt-% of graphite. Vertical slices of the X-ray tomography images of the  
5  
6  
7 polystyrene (c) and polyamide-12 (d) based electrodes having 30 wt-% of graphite.  
8  
9

10  
11  
12  
13  
14  
15 The printed electrodes can be used as electrodes for example for conventional  
16  
17  
18 electrolysis. However, in such a case the electrochemical processes take place on the  
19  
20  
21 outermost surface of the electrode (Fig. S7 and S8). The full advantage of the printed  
22  
23  
24  
25 electrodes can be obtained when they are used as flow-through electrodes for example  
26  
27  
28 in flow batteries (Fig. S9). By printing, it is possible to fine-tune the flow properties by  
29  
30  
31 adjusting the printing conditions or by printing optimized flow channels with desired  
32  
33  
34  
35 diameter and shape throughout the electrodes.  
36  
37  
38

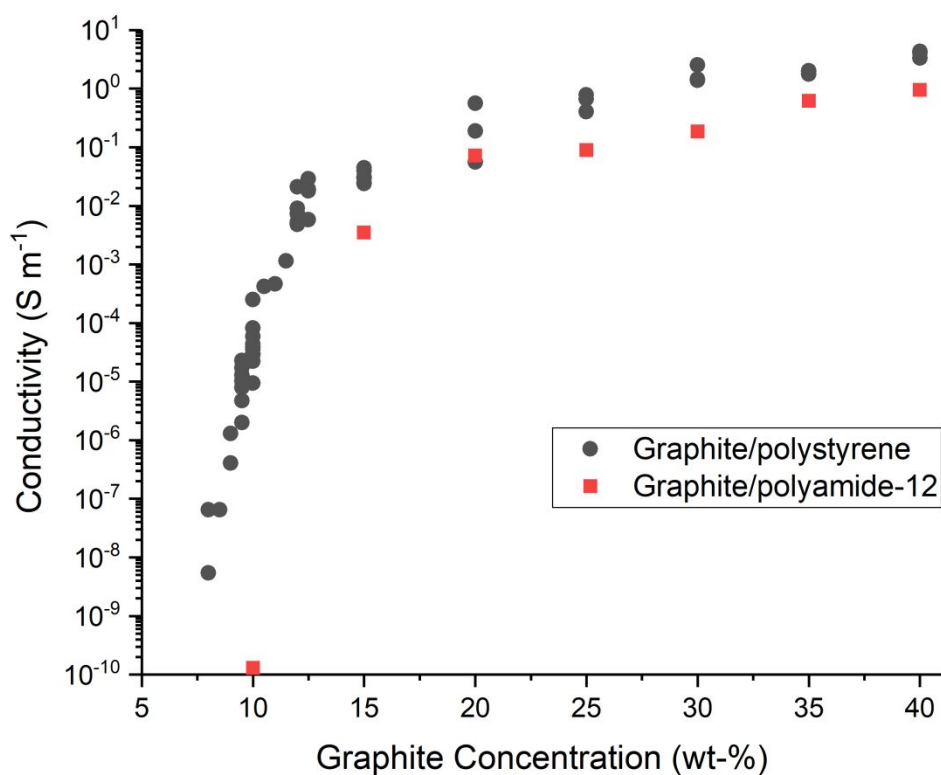
39 In addition to more rigid polystyrene and polyamide electrodes, polyurethane based  
40  
41  
42 graphite electrodes were 3D printed to obtain flexible and fully bendable, but still porous  
43  
44  
45 and conductive objects (Fig. S10). The flexible electrodes were printed using 30 wt-% of  
46  
47  
48 graphite mixed with polyurethane powder. The inherent porosity of the SLS printed  
49  
50  
51 material and the elastic nature of the polymer led to an object which conductivity could be  
52  
53  
54  
55  
56  
57  
58  
59  
60



1  
2  
3 reversibly changed by applying pressure to it (Fig. S11). When the flexible material is  
4  
5  
6  
7 compressed, the graphite particles, scattered on the surfaces of the polymer beads, are  
8  
9  
10 pressed together, which lowers the resistance and increases the conductivity. The  
11  
12  
13 change is considerable and can be easily measured. Such behavior opens up the  
14  
15  
16  
17 possibility of using the material as a simple pressure sensor or a sensor for mechanical  
18  
19  
20 stress. Even though closely related piezoresistive materials are known and widely  
21  
22  
23 reported,<sup>28-31</sup> SLS 3D printing could provide an alternative way to prepare objects with  
24  
25  
26  
27  
28 pressure/conductivity correlation.  
29  
30

31 Conductivities of the rigid electrodes were studied in detail by using a high resistance  
32  
33  
34 meter. From the conductivities of the graphite/polystyrene electrodes (Fig. 4), it can be  
35  
36  
37  
38 seen that the conductivity increases rapidly when graphite concentration is raised from  
39  
40  
41  
42 7.5 wt-% to 15 wt-% indicating that in these samples the conductivity jumps after the  
43  
44  
45 graphite concentration is high enough to produce firm graphite-graphite contacts in the  
46  
47  
48 material. It is likely that only certain chains of graphite-graphite contacts participate in the  
49  
50  
51  
52 actual conduction paths, as stated in the percolation theory.<sup>32</sup> However, the printed  
53  
54  
55  
56 electrodes contain enough of these chains to generate uniform behavior throughout the  
57  
58  
59  
60

1  
2  
3  
4 object. The increasing trend in conductivity then continues as the graphite concentration  
5  
6  
7 is increased further beyond 15 wt-%. Naturally, the highest conductivity of  $4.3 \text{ S m}^{-1}$  is  
8  
9  
10 observed with the highest concentration of graphite. Similar trend can be seen in the  
11  
12  
13 conductivities of the graphite/PA12 electrodes as they also seem to possess a rather  
14  
15  
16 sharp threshold for the conductivity between 10 and 15 wt-%. Highest observed  
17  
18  
19 conductivity was  $0.9 \text{ S m}^{-1}$ , which is considerably less than that observed for the PS based  
20  
21  
22  
23  
24 electrodes.  
25  
26  
27  
28  
29



1  
2  
3  
4 Figure 4. Conductivities of the 3D printed PS and PA12 electrodes as a function of the  
5  
6  
7 graphite concentration measured at 300 K.  
8  
9

10  
11  
12  
13  
14  
15 To obtain a reference point and a limiting maximum conductivity for the results, tightly  
16  
17  
18 packed compressed pellets were made of the graphite powder using a hydraulic press.  
19

20  
21  
22 The conductivities of the pure graphite pellets ranged between 55.1 and 70.8 S m<sup>-1</sup>. The  
23  
24  
25 conductivities observed for the 3D printed electrodes are an order of magnitude lower  
26  
27  
28 than those observed for the pure graphite pellets, but obviously, the controllable porosity,  
29  
30  
31 shape, sizes, and flow properties are not achievable by the compressed pellets.  
32  
33

34  
35  
36 The results highlight the usability of the SLS 3D printing technique in the preparation of  
37  
38  
39 highly customizable porous carbonous electrodes. It should be noted that the electrodes  
40  
41  
42 fabricated here are not optimized to obtain the maximum conductivity. Low-cost carbon  
43  
44  
45 additive with rather small inherent conductivity was utilized for the study. Meaning that  
46  
47  
48 the electric properties of the electrodes could be significantly increased by customization  
49  
50  
51 of the material itself. However, even these simple electrodes are already fully functional  
52  
53  
54  
55  
56  
57  
58  
59  
60

1  
2  
3 and can be used in electrochemical processes. It is more than likely that the full advantage  
4  
5  
6  
7 could be achieved in processes where the porosity and flow-through properties can be  
8  
9  
10 utilized. One of such potential application could be flow batteries.  
11  
12  
13  
14  
15  
16

## 17 **Discussion**

18  
19 The SLS 3D printing provides a way to easily fabricate highly customizable electrodes  
20  
21 even by using low-cost materials. The 3D printing technique gives the possibility to fine-  
22  
23 tune the mechanical parameters such as the porosity and the flexibility of the electrodes  
24  
25  
26 by altering the supporting matrix material and the printing conditions. The technique is  
27  
28  
29 able to produce durable electrodes with high porosity and sufficient conductivity  
30  
31 compared to the bulk graphite. Even though the study focused on graphite as the additive  
32  
33  
34 and common polymers as matrices, the method is not limited to these to materials and  
35  
36  
37 could be expanded to use different additives and polymers.  
38  
39  
40  
41  
42  
43  
44  
45  
46

47 By using other additives such as conductive polymers or other carbon sources, or  
48  
49 maybe even metals as well as choosing other types of supporting matrices, including  
50  
51  
52 conductive materials, the properties of the printed electrodes could be tuned and  
53  
54  
55  
56  
57  
58  
59  
60

1  
2  
3 enhanced further. The possibility to tailor and design highly porous electrodes with well-  
4  
5  
6 defined conductivity and flow-properties could open up a whole new way of fabricating  
7  
8  
9  
10 highly efficient electrodes.  
11  
12  
13  
14  
15  
16

## 17 **Experimental Section**

### 20 **Materials**

21  
22  
23  
24 The graphite used for preparation of the starting material was synthetic graphite powder  
25  
26  
27 (<20  $\mu\text{m}$ ) purchased from Sigma Aldrich. The polymer powders with average particle  
28  
29  
30 diameters of 50  $\mu\text{m}$  were purchased from ADVANC3D Materials. All chemicals were used  
31  
32  
33  
34  
35 as received.  
36  
37  
38  
39  
40  
41

### 42 **Three-dimensional printing**

43  
44  
45 The 3D-models of electrodes were designed using FreeCAD v.0.16 software after which  
46  
47  
48 they were sliced into two dimensional, 0.1 mm thick, slices using Slic3r v. 1.2.9.  
49  
50  
51  
52 Electrodes were printed with Sharebot SnowWhite SLS 3D printer. For preparation of the  
53  
54  
55  
56 polystyrene based electrodes, laser speed was varied between 200  $\text{mm s}^{-1}$  and 1200 mm  
57  
58  
59  
60

1  
2  
3  
4 s<sup>-1</sup>, depending on the amount of graphite in the mixture, with powder temperatures  
5  
6  
7 between 106 and 108 °C and CO<sub>2</sub> laser power of 14 W. For polyurethane, similar settings  
8  
9  
10 were used but temperature was set to 121 °C. Polyamide-12 based electrodes were  
11  
12  
13 fabricated using laser speeds varying between 360 mm s<sup>-1</sup> and 2560 mm s<sup>-1</sup> and  
14  
15  
16 temperatures between 160 and 167 °C with laser power varying between 4 W and 14 W.  
17  
18  
19  
20  
21 The 3D printing settings were adjusted for different graphite contents to obtain sufficient  
22  
23  
24 mechanical properties. The printed objects were carefully cleaned of all unsintered  
25  
26  
27 powder before using them in experiments.  
28  
29  
30  
31  
32  
33  
34  
35  
36  
37

### 38 **Helium Ion Microscopy and Scanning Electron Microscopy**

39  
40  
41  
42 Helium Ion Microscopy was performed using Carl Zeiss ORION NanoFab. The beam  
43  
44  
45 energy used was around 30 kV with beam current ranging from 0.242 to 0.303 pA. Scan  
46  
47  
48 dwell time of 0.2 μs was used. Flood gun was used to counteract the charging effect. For  
49  
50  
51  
52 HIM imaging samples did not receive any additional pretreatment after the 3D printing  
53  
54  
55 process. Scanning electron microscopy was done using Zeiss EVO-50XVP with  
56  
57  
58  
59  
60

1  
2  
3 accelerating voltage of 25 kV. Prior to SEM imaging the 3D printed electrodes were  
4  
5  
6  
7 coated with gold for optimal picture quality.  
8  
9

### 14 **X-ray tomography**

15  
16  
17 X-ray tomographic imaging of the electrodes was carried out using SkyScan 1172  
18  
19  
20  
21 microtomograph. Two cylinder shaped samples of 4-5 mm in diameter were imaged with  
22  
23  
24 3.0  $\mu\text{m}$  pixel size. The scanning parameters for both samples were identical. The X-ray  
25  
26  
27  
28 source parameters were 29 kV and 100  $\mu\text{A}$  and no filter was used. A total of 1200  
29  
30  
31 projection images were taken using 0.3 degree step size over 360 degree of rotation.  
32  
33  
34  
35 Projection images were averaged over 4 exposures of 4712 ms resulting in a total  
36  
37  
38 exposure time of 18.85 s for each of them. A total scan duration was 8 hours.  
39  
40  
41  
42 Tomographic images were reconstructed using NRecon software, which is based on  
43  
44  
45 Feldkamp algorithm.<sup>33</sup> One pixel post-alignment was needed for ideal reconstruction. No  
46  
47  
48 ring artifact correction or beam hardening correction was used. A total sample height that  
49  
50  
51  
52 was reconstructed was 5.6 mm for both samples. To measure the relative porosity of the  
53  
54  
55  
56 samples, the volumes of the pore structures and the total volumes of the samples were  
57  
58  
59  
60

1  
2  
3 analyzed from the X-ray tomography images similarly, using ImageJ software. Additional  
4  
5  
6  
7 information about the analysis is presented in supplementary information.  
8  
9

### 10 11 12 13 14 **Conductivity measurements** 15

16  
17 Keithley 6517A Electrometer/High resistance meter was used to measure the  
18  
19  
20  
21 resistance at room temperature. An attempt to minimize contact resistance was done by  
22  
23  
24 connecting copper plates to the sample with carbon black paste. Xylene was used as a  
25  
26  
27 solvent in carbon black paste. Copper wires were soldered to the plates and the wires  
28  
29  
30  
31 were ran into the measuring apparatus. Copper plates were scratched with sand paper  
32  
33  
34 to get rid of oxide layer and to increase the contact area. High resistance samples were  
35  
36  
37  
38 also soldered inside a shielded box so that coaxial wires came out of the box and were  
39  
40  
41  
42 connected to the apparatus. Carbon black paste was applied as viscous as possible to  
43  
44  
45 prevent the paste from entering the pores of the material.  
46  
47  
48  
49  
50  
51

52 *Supporting information. Detailed description of X-ray tomography analysis as well as*  
53  
54  
55  
56 *Pore structure distribution graphs, Additional SEM images, Images of 3D printed*  
57  
58  
59  
60



1  
2  
3  
4 *electrodes being used for electrolysis and in a flow cell, Images of flexible 3D printed*  
5  
6  
7 *electrodes.*  
8  
9

## 11 AUTHOR INFORMATION

### 15 Corresponding Author

18  
19 \* Prof. M. Haukka

20  
21  
22 Department of Chemistry, University of Jyväskylä, P.O. Box 35, FI-40014 Jyväskylä,  
23  
24  
25 Finland

26  
27  
28 Email: [matti.o.haukka@jyu.fi](mailto:matti.o.haukka@jyu.fi)  
29

### 31 Author Contributions

32  
33  
34  
35  
36 M.H. conceptualized the idea of the SLS 3D printed electrodes. E.L. and E.K. did the  
37  
38  
39  
40 designing and the 3D printing of the electrodes. J.J. performed the conductivity  
41  
42  
43 experiments for the electrodes. M.A. supervised the conductivity measurements. J.P. and  
44  
45  
46  
47 J.V. performed the X-ray tomography and the analysis of the results. L.K. assisted in the  
48  
49  
50 design and fabrication of the flexible electrodes. E.L. wrote the initial manuscript which  
51  
52  
53  
54 was jointly revised.  
55  
56  
57  
58  
59  
60

## Competing Interests

The authors declare no competing interests.

## Data Availability

The data supporting the findings of this study is available from the corresponding author upon reasonable request.

## Acknowledgments

Financial support from the Centennial Foundation of Technology industries of Finland and Jane and Aatos Erkko foundation is greatly appreciated. The research was also supported by Academy of Finland (grant number: 295581 (M.H.)) and University of Jyväskylä.

## References

- (1) Armand, M.; Tarascon, J.-M. Building Better Batteries. *Nature* **2008**, *451*, 652–657.
- (2) Larcher, D.; Tarascon, J.-M. Towards Greener and More Sustainable Batteries for Electrical Energy Storage. *Nat. Chem.* **2015**, *7*, 19–29.
- (3) Aricò, A. S.; Bruce, P.; Scrosati, B.; Tarascon, J.-M.; van Schalkwijk, W. Nanostructured Materials for Advanced Energy Conversion and Storage Devices. In *Materials for Sustainable Energy*, 2010; pp 148–159.
- (4) Kim, K. S.; Zhao, Y.; Jang, H.; Lee, S. Y.; Kim, J. M.; Kim, K. S.; Ahn, J.-H.; Kim, P.; Choi, J.-Y.; Hong, B. H. Large-Scale Pattern Growth of Graphene Films for Stretchable Transparent Electrodes. *Nature* **2009**, *457*, 706–710.
- (5) Wang, F.; Wu, X.; Yuan, X.; Liu, Z.; Zhang, Y.; Fu, L.; Zhu, Y.; Zhou, Q.; Wu, Y.; Huang, W. Latest Advances in Supercapacitors: From New Electrode Materials to Novel Device Designs. *Chem. Soc. Rev.* **2017**, *46*, 6816–6854.
- (6) Li, B.; Nie, Z.; Vijayakumar, M.; Li, G.; Liu, J.; Sprenkle, V.; Wang, W. Ambipolar

- 1  
2  
3  
4 Zinc-Polyiodide Electrolyte for a High-Energy Density Aqueous Redox Flow  
5  
6  
7 Battery. *Nat. Commun.* **2015**, *6*, 6303.  
8  
9  
10  
11 (7) Bruce, P. G.; Scrosati, B.; Tarascon, J.-M. Nanomaterials for Rechargeable Lithium  
12  
13  
14 Batteries. *Angew. Chemie Int. Ed.* **2008**, *47*, 2930–2946.  
15  
16  
17  
18  
19 (8) Cho, C.-Y.; Moon, J. H. Hierarchically Porous TiO<sub>2</sub> Electrodes Fabricated by Dual  
20  
21  
22 Templating Methods for Dye-Sensitized Solar Cells. *Adv. Mater.* **2011**, *23*, 2971–  
23  
24  
25  
26  
27 2975.  
28  
29  
30  
31 (9) Yoon, S.; Oh, S. M.; Lee, C. W.; Ryu, J. H. Pore Structure Tuning of Mesoporous  
32  
33  
34 Carbon Prepared by Direct Templating Method for Application to High Rate  
35  
36  
37 Supercapacitor Electrodes. *J. Electroanal. Chem.* **2011**, *650*, 187–195.  
38  
39  
40  
41  
42 (10) Doherty, C. M.; Caruso, R. A.; Smarsly, B. M.; Drummond, C. J. Colloidal Crystal  
43  
44  
45 Templating to Produce Hierarchically Porous LiFePO<sub>4</sub> Electrode Materials for High  
46  
47  
48 Power Lithium Ion Batteries. *Chem. Mater.* **2009**, *21*, 2895–2903.  
49  
50  
51  
52  
53 (11) Park, J.; Lee, W. H.; Huh, S.; Sim, S. H.; Kim, S. Bin; Cho, K.; Hong, B. H.; Kim, K.  
54  
55  
56  
57  
58  
59  
60

- 1  
2  
3  
4 S. Work-Function Engineering of Graphene Electrodes by Self-Assembled  
5  
6  
7 Monolayers for High-Performance Organic Field-Effect Transistors. *J. Phys. Chem.*  
8  
9  
10 *Letf.* **2011**, *2*, 841–845.  
11  
12  
13  
14  
15 (12) Yip, H.-L.; Hau, S. K.; Baek, N. S.; Ma, H.; Jen, A. K.-Y. Polymer Solar Cells That  
16  
17  
18 Use Self-Assembled-Monolayer- Modified ZnO/Metals as Cathodes. *Adv. Mater.*  
19  
20  
21 **2008**, *20*, 2376–2382.  
22  
23  
24  
25  
26 (13) Ambrosi, A.; Pumera, M. 3D-Printing Technologies for Electrochemical  
27  
28  
29 Applications. *Chem. Soc. Rev.* **2016**, *45*, 2740–2755.  
30  
31  
32  
33  
34 (14) Fu, K.; Yao, Y.; Dai, J.; Hu, L. Progress in 3D Printing of Carbon Materials for  
35  
36  
37 Energy-Related Applications. *Adv. Mater.* **2017**, *29*, 1603486.  
38  
39  
40  
41  
42 (15) Sun, K.; Wei, T.-S.; Ahn, B. Y.; Seo, J. Y.; Dillon, S. J.; Lewis, J. A. 3D Printing of  
43  
44  
45 Interdigitated Li-Ion Microbattery Architectures. *Adv. Mater.* **2013**, *25*, 4539–4543.  
46  
47  
48  
49  
50 (16) Fu, K.; Wang, Y.; Yan, C.; Yao, Y.; Chen, Y.; Dai, J.; Lacey, S.; Wang, Y.; Wan, J.;  
51  
52  
53  
54 Li, T.; et al. Graphene Oxide-Based Electrode Inks for 3D-Printed Lithium-Ion  
55  
56  
57  
58  
59  
60

- 1  
2  
3 Batteries. *Adv. Mater.* **2016**, *28*, 2587–2594.  
4  
5  
6  
7
- 8 (17) García-Tuñón, E.; Barg, S.; Franco, J.; Bell, R.; Eslava, S.; D'Elia, E.; Maher, R. C.;  
9  
10  
11 Guitian, F.; Saiz, E. Printing in Three Dimensions with Graphene. *Adv. Mater.* **2015**,  
12  
13  
14  
15 *27*, 1688–1693.  
16  
17  
18
- 19 (18) Reyes, C.; Somogyi, R.; Niu, S.; Cruz, M. A.; Yang, F.; Catenacci, M. J.; Rhodes,  
20  
21  
22  
23 C. P.; Wiley, B. J. Three-Dimensional Printing of a Complete Lithium Ion Battery  
24  
25  
26 with Fused Filament Fabrication. *ACS Appl. Energy Mater.* **2018**, *1*, 5268–5279.  
27  
28  
29
- 30 (19) Maurel, A.; Courty, M.; Fleutot, B.; Tortajada, H.; Prashantha, K.; Armand, M.;  
31  
32  
33  
34 Grugeon, S.; Panier, S.; Dupont, L. Highly Loaded Graphite–Polylactic Acid  
35  
36  
37  
38 Composite-Based Filaments for Lithium-Ion Battery Three-Dimensional Printing.  
39  
40  
41  
42 *Chem. Mater.* **2018**, *30*, 7484–7493.  
43  
44  
45
- 46 (20) Yao, B.; Chandrasekaran, S.; Zhang, J.; Xiao, W.; Qian, F.; Zhu, C.; Duoss, E. B.;  
47  
48  
49  
50 Spadaccini, C. M.; Worsley, M. A.; Li, Y. Efficient 3D Printed Pseudocapacitive  
51  
52  
53  
54 Electrodes with Ultrahigh MnO<sub>2</sub> Loading. *Joule* **2018**.  
55  
56  
57  
58  
59  
60

- 1  
2  
3  
4 (21) Shi, D.; Gibson, I. Material Properties and Fabrication Parameters in Selective  
5  
6  
7 Laser Sintering Process. *Rapid Prototyp. J.* **1997**, *3*, 129–136.  
8  
9  
10  
11 (22) Shirazi, S. F. S.; Gharehkhani, S.; Mehrali, M.; Yarmand, H.; Metselaar, H. S. C.;  
12  
13  
14 Adib Kadri, N.; Osman, N. A. A. A Review on Powder-Based Additive Manufacturing  
15  
16  
17 for Tissue Engineering: Selective Laser Sintering and Inkjet 3D Printing. *Sci.*  
18  
19  
20  
21  
22 *Technol. Adv. Mater.* **2015**, *16*, 33502.  
23  
24  
25  
26 (23) Fina, F.; Goyanes, A.; Gaisford, S.; Basit, A. W. Selective Laser Sintering (SLS) 3D  
27  
28  
29  
30  
31  
32  
33  
34  
35 (24) Dizon, J. R. C.; Espera, A. H.; Chen, Q.; Advincula, R. C. Mechanical  
36  
37  
38  
39  
40  
41  
42  
43 (25) Lahtinen, E.; Hänninen, M. M.; Kinnunen, K.; Tuononen, H. M.; Väisänen, A.;  
44  
45  
46  
47  
48  
49  
50  
51  
52  
53  
54  
55  
56  
57  
58  
59  
60
- 1800048.

- 1  
2  
3  
4 (26) Novák, P.; Müller, K.; Santhanam, K. S. V.; Haas, O. Electrochemically Active  
5  
6  
7 Polymers for Rechargeable Batteries. *Chem. Rev.* **1997**, *97*, 207–282.  
8  
9  
10  
11 (27) Joens, M. S.; Huynh, C.; Kasuboski, J. M.; Ferranti, D.; Sigal, Y. J.; Zeitvogel, F.;  
12  
13  
14 Obst, M.; Burkhardt, C. J.; Curran, K. P.; Chalasani, S. H.; et al. Helium Ion  
15  
16  
17 Microscopy (HIM) for the Imaging of Biological Samples at Sub-Nanometer  
18  
19  
20  
21  
22 Resolution. *Sci. Rep.* **2013**, *3*, 3514.  
23  
24  
25  
26 (28) Konarova, M.; Aslam, W.; Ge, L.; Ma, Q.; Tang, F.; Rudolph, V.; Beltramini, J. N.  
27  
28  
29 Enabling Process Intensification by 3D Printing of Catalytic Structures.  
30  
31  
32  
33 *ChemCatChem* **2017**, *9*, 4132–4138.  
34  
35  
36  
37 (29) Petchartee, S.; Monkman, G. Optimisation of Prehension Force through Tactile  
38  
39  
40  
41 Sensing. *Ind. Rob.* **2008**, *35*, 361–368.  
42  
43  
44  
45 (30) Russel, A. R. *Robot Tactile Sensing*, Prentice-Hall: Australia, 1990.  
46  
47  
48  
49  
50 (31) Yaniger, S. I. Force Sensing Resistors: A Review Of The Technology. In *Electro*  
51  
52  
53  
54 *International*, 1991; 1991; pp 666–668.  
55  
56  
57  
58  
59  
60



- 1  
2  
3  
4 (32) Kalaitzidou, K.; Fukushima, H.; Drzal, T. L. A Route for Polymer Nanocomposites  
5  
6  
7 with Engineered Electrical Conductivity and Percolation Threshold. *Materials* .  
8  
9  
10 2010.  
11  
12  
13  
14  
15 (33) Feldkamp, L. A.; Davis, L. C.; Kress, J. W. Practical Cone-Beam Algorithm. *J. Opt.*  
16  
17  
18 *Soc. Am. A* 1984, 1, 612–619.  
19  
20  
21  
22  
23  
24  
25  
26  
27

28 **Table of Content Entry:**  
29

